Creep of Pure Materials and Alloys

W. Blum, S. Straub and S. Vogler

Institut für Werkstoffwissenschaften, Lehrstuhl I
Universität Erlangen-Nürnberg
Martensstraße 5, D-W-8520 Erlangen, Germany

CONTENTS

Abstract

The steady-state dislocation structure that develops during creep is a subgrain structure. The characteristic dislocation spacings are mainly determined by stress. The kinetics of deformation are different for steady-state deformation and at constant dislocation structure. This is explained on the basis of two mechanisms of dislocation motion which are coupled by internal stresses: glide of free dislocations in the subgrain interior and motion of subgrain boundaries. For pure materials the parameters of the model can be related to the characteristic dislocation spacings. For alloys the deformation kinetics are strongly influenced by solute and particle hardening.

1. Introduction

Plastic deformation tends towards a *steady state* of dynamic equilibrium between generation and annihilation of dislocations. Since the early work of Sherby, Dorn and coworkers there is a general conviction that steady-state deformation at high temperatures is related to diffusion (see the reviews of Sherby and Burke /1/, Bird, Mukherjee and Dorn /2/ and Nix and Ilschner /3/). This relation can be derived in a simple manner as follows: Assume that diffusion of matter over a distance d between sources and sinks in a volume element d^3 controls deformation. The rate $\dot{d}$ at which the length of the volume element changes with time is given as the product of the mobility of atoms, D/k_BT (D: coefficient of self diffusion, k_B: Boltzmann constant, and T: temperature), and the average gradient of the potential, $\Omega\sigma/(d/c_1)$ (Ω: atomic volume, σ: normal stress, and $c_1 \geq 1$: numerical constant). The tensile strain rate is $\dot{\varepsilon} = \dot{d}/d$. Setting $d = d_g$, where d_g is the grain size, one obtains the expression for diffusive flow via vacancies /4/:

$$\dot{\epsilon} \approx c_1 \frac{D\Omega\sigma}{k_B T d_g^2} \qquad (1)$$

Setting d equal to the average dislocation spacing $\rho^{-0.5}$ (ρ: length of dislocation lines per volume), using the experimental relation between dislocation spacing and shear-modulus (G) normalised (normal) stress σ, $\rho^{-0.5} \sim bG/\sigma$ (b: length of Burgers vector) and expressing Ω as b^3, one gets (with $c_1 \approx 1$) what Weertman /5/ has called the natural creep law:

$$\dot{\epsilon} \approx \frac{D\Omega\sigma}{k_B T(\rho^{-0.5})^2} \approx \frac{DGb}{k_B T}\left(\frac{\sigma}{G}\right)^3 \qquad (2)$$

with a third power stress dependence.

The steady state of deformation is preceded by a *transient* stage. The description of transient deformation by Alexander and Haasen /6/ is based on the Orowan equation, $\dot{\gamma} = b\rho v$ (γ: shear strain, v: average dislocation velocity), and a phenomenological relation $v = v_0 \tau^{*m}$ (m = const) between v and the resolved shear stress component τ^* available for dislocation motion. Throughout this work we will relate shear and tensile stresses and strains by $M = \sigma/\tau = d\gamma/d\varepsilon$, where $M \geq 2$ is an appropriate geometrical factor (Taylor factor or inverse of Schmid factor). $\tau^* = \tau - \tau_G$ is smaller than the total applied stress τ by an athermal stress component τ_G, which in turn increases with decreasing dislocation spacing $\rho^{-0.5}$ as $\tau_G = \alpha Gb\rho^{0.5}$ with constant α. Thus:

$$\dot{\gamma} = b\rho v_0(\tau - \alpha Gb\rho^{0.5})^m \qquad (3)$$

This "kinetic law" predicts a point of minimum deformation resistance (relative maximum of $\dot{\gamma}$ at constant τ and relative minimum of τ ("lower yield stress") at constant $\dot{\gamma}$) for a certain value $\rho_{extr}^{-0.5}$ of the dislocation spacing depending on stress according to:

$$\rho_{extr}^{-0.5} = \alpha\left(1 + \frac{m}{2}\right) bG/\tau \qquad (4)$$

For $m \approx 1$, $\rho_{extr}^{-0.5}$ may be smaller than the steady-state spacing of dislocations. This means that the point of minimum deformation resistance is approached, but not reached in the transient range of deformation at constant stress when $\rho^{-0.5}$ decreases implying that the strain rate $\dot{\gamma}$ at constant τ varies in the same direction as the dislocation *density*. This is called *inverted transient*

deformation. During *normal transient* deformation $\dot{\gamma}$ varies in the same direction as the dislocation *spacing*, because m >> 1 so that $\rho^{-0.5}$ is much larger than the steady-state spacing of dislocations and the steady state is reached long after the point of minimum deformation resistance. Thus the simple kinetic law (3) based on a single mechanism of dislocation motion gives a simple microstructural explanation of the difference in transient deformation behaviour of the classes M (pure materials with m >> 1) and A (strongly solute hardened alloys with m ≈ 1) of materials.

Creep resistant engineering materials are generally strengthened by solutes and/or particles. Solute strengthening damps the hectic transient deformation response of pure materials by shifting it from the normal (work hardening) to the inverted (work softening) type. The simplest way to account for particle strengthening is to diminish the applied stress σ by a particle hardening term σ_p. The difficulty is to derive the right value for σ_p, which decreases with decreasing stress due to different mechanisms of thermal activated overcoming of particles (see, for example, Blum and Reppich /7/ and Reppich /8/).

In the final stages of creep nucleation and growth of pores lead to fracture /9/. Often the so-called tertiary stage of creep, in which the creep rate increases continuously with strain (and time) from its minimum value $\dot{\varepsilon}_{min}$ in the secondary stage, is identified with damage due to pores. However, as we will show below for a ferritic steel, this is not always true because other mechanisms of softening are limiting the secondary stage of creep. It is generally sufficient to relate the time to fracture t_{fr} to ε_{min} via a fracture strain ε_{fr} according to the Monkman-Grant relation:

$$t_{fr} = \int_0^{t_{fr}} dt = \int_0^{\epsilon_{fr}} \frac{d\epsilon}{\dot{\epsilon}(\epsilon)} = \frac{1}{\dot{\epsilon}_{min}} \int_0^{\epsilon_{fr}} \frac{d\epsilon}{\dot{\epsilon}/\dot{\epsilon}_{min}} = \frac{C_{MG}}{\dot{\epsilon}_{min}} \quad (5)$$

where C_{MG} is a constant (Monkman-Grant constant), because the ratio $\dot{\varepsilon}/\dot{\varepsilon}_{min}$ is to a first approximation independent of stress and temperature near $\dot{\varepsilon}_{min}$.

We conclude this quick overview by noting that one of the most important tasks in the field of creep and high temperature deformation in general is to understand the dynamics of the microstructural development, in particular that of the dislocation structure, and its relation to the kinetics of deformation. In this contribution we will describe the dislocation structure (section 2) and the kinetics of deformation (section 3) and finally consider the quantitative description of deformation based on microstructure (section 4).

2. Dislocation Structure

A. Subgrain Formation

An elementary step of glide inside a crystal is necessarily connected with internal stresses. The crystal tries to relax these stresses. This can be done in two ways /12/, either by polygonization or by secondary slip (Fig. 2). Polygonization means that the sheared volume grows, until it extends through the whole crystal so that it is free to rotate, creating a polygonized surface trace. The region between two polygonized plates is a kink band (Fig. 2a). It is made up from walls of edge dislocations of opposite sign. Fig. 1 shows a kink band in Cu single crystals deformed at elevated temperature. In the alternative process, slip on a second slip system allows the volume between two slipped regions to change its shape and to rotate (Fig. 2b). This leads to relaxation of long-range stresses as is evident from the fact that an isolated subgrain has formed. If two slip systems are equally active, polygonization occurs on both systems. The intersection of deformed plates leads to a box structure, with misorientations of opposite sign between the boxes (Fig. 2c, 3). With increasing strain more than two slip systems take part in deformation and the subgrain structure becomes equiaxed.

Subgrain formation is a fundamental process of dislocation patterning not only in pure crystalline materials, but also in solid solution and particle-hardened alloys /13/. This statement seems to be in conflict with experimental observations on strongly solute hardened alloys (see the review by Oikawa and Langdon /14/). However, it must be noted that the steady state of the dislocation structure may be attained distinctly later than the (approximate) steady state of deformation resistance,

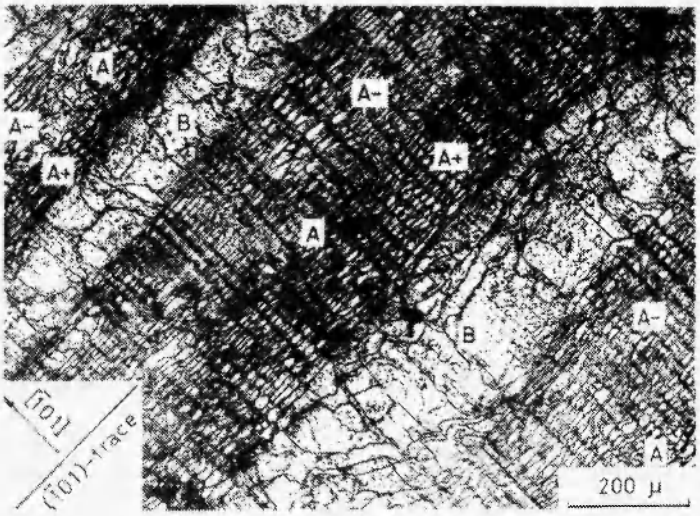

Fig. 1: Kink band in Cu single crystal deformed in single glide mode at 745 °C corresponding to Fig. 2a, from Hasegawa et al. /10/.

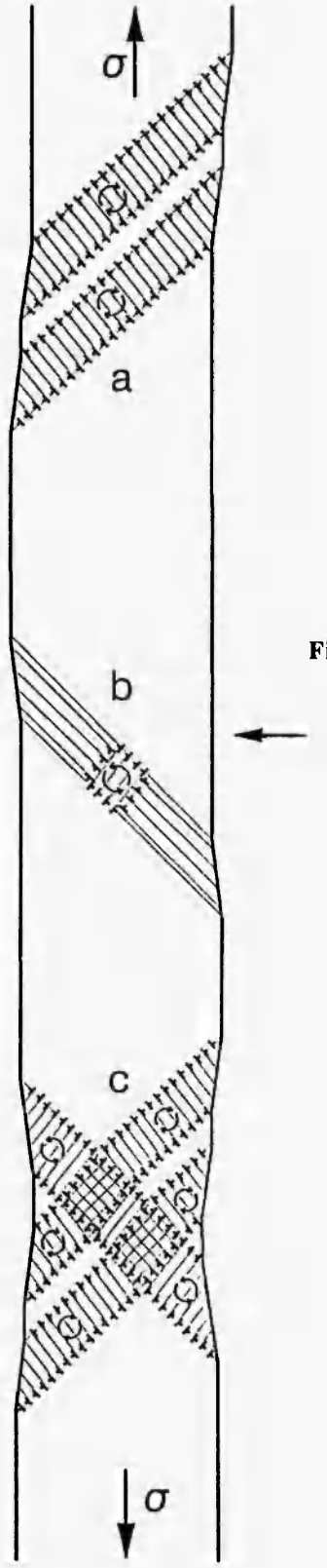

Fig. 2: Formation of subgrains by combined deformation and lattice rotation (indicated by arrows): a) Elongated subgrains with kink band in between; b) Isolated subgrain formed by secondary slip; c) Superposition of elongated subgrains from two slip systems.

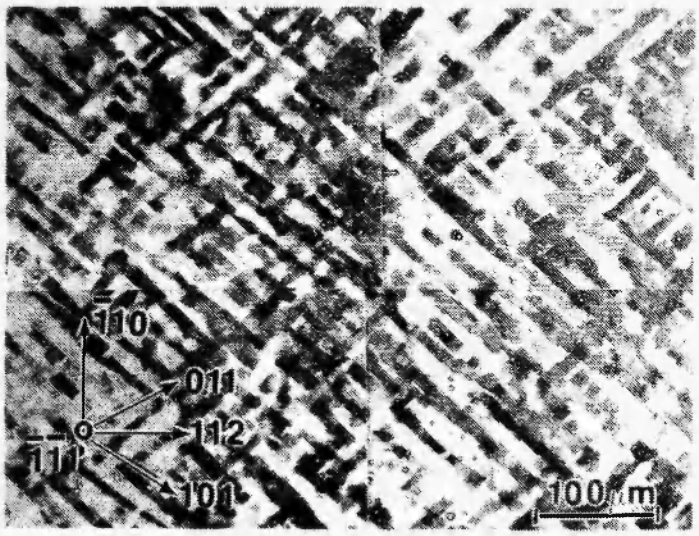

Fig. 3: Box structure in Al single crystal deformed in double glide mode at 150 °C corresponding to Fig. 2c, from Carrard and Martin /11/.

so that subgrain formation may easily be overlooked. For instance, if the steady-state dislocation spacing is close to $\rho_{extr}^{-0.5}$ (Eq. 4), there may be no observable change in deformation resistance although the steady-state dislocation structure has not yet been attained. Formation of subgrains requires strain. For a Ni-base alloy it was reported /15/ that the strain to fill 50% of the volume with subgrains increases in proportion to stress as $\varepsilon_{sub,50\%} = 52\ \sigma/G$.

B. Characteristic Dislocation Spacings

The three main length characteristics of the dislocation structure are the average spacings of subgrain boundaries (w), "free" dislocations in the subgrain interior ($\rho_f^{-0.5}$), and dislocations in subgrain boundaries (s). w is determined by the line intersection method. ρ_f is obtained from the points of intersection of dislocation lines with the cross section of the subgrain interior. The determination of s is problematical /13/, due to the variations of the spacings of families of parallel dislocations in one boundary and from boundary to boundary. Often, the misorientation angle θ is measured and assumed to be related to s by $s \approx b/\theta$. In pure materials the dislocation spacings depend mainly on stress σ normalized by the shear modulus G (= $[c_{44}(c_{11} - c_{12})]^{0.5}$ for cubic crystals where c_{ik} are the elastic constants). Figs. 4a and 4b show the relations between dislocation spacings and normalized stress in the steady state of deformation of pure NaCl (M = 2) and pure Al (M = 3). In both cases the subgrain size is inversely proportional to stress:

$$w = \alpha_w bG/\tau_G = c_2 bG/\sigma$$
$$c_2 = \alpha_w M\sigma/\sigma_G \qquad (6)$$

where c_2 equals 35 for NaCl and 28 for Al. The value of c_2 seems to decrease with decreasing stacking fault energy. The average value for a number of materials is 23 /17/. It is believed that the relation between w and applied stress σ results from the relation between w and the athermal shear stress component τ_G, which in turn is related to some average dislocation spacing. It seems noteworthy that the length d_{sl} of slip lines, which have been observed /18/ at the surface of NaCl single crystals during work hardening at constant strain rate $\dot{\varepsilon}$ at room temperature in stages II and III, is of the same order as the subgrain size (Fig. 4a). A similar relationship has been found between the length of slip lines and the size of cells during work hardening of Cu single crystals /19/. It appears that cell boundaries during work hardening as well as subgrain boundaries during steady-state deformation are obstacles to slip of free dislocations. In fact, slip lines have been observed to end preferentially at subgrain boundaries /20/. In his areal glide model, Kocks /21/ interprets the size of cells as the spacing of "hard spots" in the glide plane.

The stress dependence of $\rho_f^{-0.5}$ is expressed in a manner analogous to that of w:

$$\rho_f^{-0.5} = \alpha_f bG/\tau_{G,f} = c_3 bG/\sigma$$
$$c_3 = \alpha_f M\sigma/\sigma_{G,f} \qquad (7)$$

As shown in Fig. 4a for NaCl, c_3 is of order 1. (The fact that the steady-state values of $\rho_f^{-0.5}$ level off at about 1 μm is probably an artefact due to insufficient resolution of etch pits in the optical microscope.) $\tau_{G,f}$ and $\sigma_{G,f} \le \sigma_G \le \sigma$ are the athermal components of the shear stress and the normal stress, respectively, due to free dislocations. It follows from the value of c_3 that the dislocation interaction constant $\alpha_f \le c_3/M = 1/2$ for NaCl (M = 2). Fig. 4a includes the dislocation spacings $\rho_{tot}^{-0.5}$ measured during room temperature work hardening of NaCl single crystals in stages II and III at constant $\dot{\varepsilon}$ /22,23/. ρ_{tot} is the total length of dislocations per volume; the factor of converting etch pit densities into ρ_{tot} was chosen as 2. The two kinds of spacings, $\rho_{tot}^{-0.5}$ and $\rho_f^{-0.5}$, are of similar magnitude at the same σ/G. This indicates that the values of the interaction constant and the ratio $\sigma_{G,f}/\sigma$ in the cases of work hardening at room temperature and steady state deformation at high temperature are not very different.

The average spacing s of dislocations in subgrain boundaries in Al and AlZn (Fig. 4b) is less strongly dependent on stress than the other two spacings. It usually lies in a range corresponding to misorientations θ between 0.5° and 2°. There is a tendency for s to

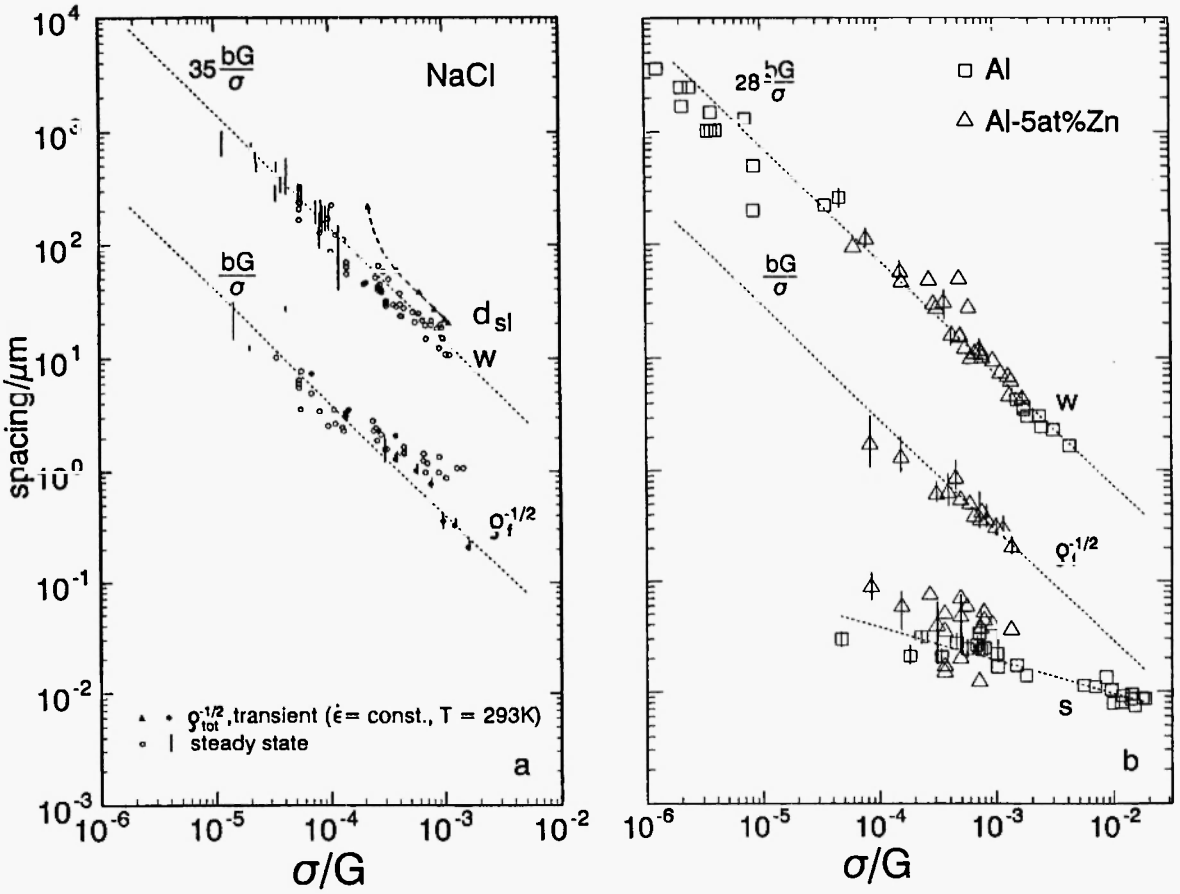

Fig. 4: Characteristic dislocation spacings w, $\rho_f^{-0.5}$ and s as a function of normalized stress for steady-state deformation of a) NaCl ($M = 2$) collected by Vogler /16/ and b) Al and AlZn ($M = 3$) /13/.
a) includes dislocation spacings and slip line lengths during room temperature work hardening at constant $\dot{\varepsilon}$.

increase with decreasing temperature and increasing stress.

To the authors' knowledge there is no pure material with a complete set of data for the dislocation spacings in a wide range of stresses. One difficulty is that $\rho_f^{-0.5}$ cannot be reliably determined in pure materials by TEM due to high mobility of free dislocations. However, in the weakly solute hardened alloy Al-5 at%Zn the structure of free dislocations can be frozen in by cooling under load. The dislocation spacings in AlZn (from TEM, Fig. 4b) are close to those found in NaCl (from etch pits, Fig. 4a), indicating that the dislocation spacings in AlZn are representative of that in pure Al under stress. Combining the ρ_f-data of AlZn with w- and s-data of Al allows to determine the ratio of the densities of free and of subgrain boundary dislocations $\rho_b = (2/s)(2/w)$. In the stress range from $6 \cdot 10^{-5}G$ to $1.4 \cdot 10^{-3}G$ the ratio ρ_f/ρ_b varies from 0.6 to 1.

In solute and particle-hardened materials the dislocation spacings are to a first approximation similar to those in pure materials. A closer look reveals certain differences. These can best be rationalized by considering the different stress components. For simplicity we assume linear additivity of the stress components. Thus

we can write:

$$\sigma = \sigma_G + \sigma^*$$
$$\sigma_G = \sigma_{G,f} + \sigma_{G,b} + \sigma_{G,p} \quad (8)$$
$$\sigma^* = \sigma_\perp^* + \sigma_{sol}^*$$

where the athermal stress component σ_G is the sum of the contributions from free dislocations ($\sigma_{G,f}$), subgrain boundaries ($\sigma_{G,b}$: long-range back stress due to subgrain boundaries), and hard particles ($\sigma_{G,p}$) and σ^* is the sum of the strongly strain-rate dependent components necessary for thermally activated glide past obstacles ($\sigma_\perp^*$) and solute friction (σ_{sol}^*). As σ_{sol}^*/σ increases strongly with increasing stress in solute hardened alloys like AlMg, the ratios σ_G/σ and $\sigma_{G,f}/\sigma$ decrease, so that according to Eqs. 6 and 7 the spacings w and $\rho_f^{-0.5}$ are larger in solute hardened alloys than in pure metals for steady-state deformation at the same shear-modulus normalized stress /13/.

In particle-hardened materials the spacing of free dislocations is again larger than in pure materials at the same normalized stress, because $\sigma_{G,f}/\sigma$ is reduced by the particle hardening term $\sigma_{G,p}$ /15,24/ in addition to the solute hardening term. However, in contrast to solid solutions the subgrain size w is generally smaller in particle-hardened materials compared to pure materials at the same normalized stress. This suggests that formation of subgrains is initiated not only by free dislocations, but also by particles, and that w is determined by the sum of $\sigma_{G,f} + \sigma_{G,p} \approx \sigma_G$, consistent with Eq. 6. It follows from the suppression of the density of free dislocations by particle hardening that the ratio ρ_f/ρ_b may be quite low in particle-hardened alloys: From the set of data for NiCr22Co12Mo9 published in An et al. /15/ one finds that ρ_f/ρ_b falls from 1.6 at $\sigma = 5 \cdot 10^{-3}G$ to a small value of only 0.06 at a relatively small stress of $\sigma = 1.5 \cdot 10^{-3}G$.

C. Grain Boundary Migration

A striking structural feature is that the subgrains remain equaxed even at extremely high strains and high strain rates during hot working. Exell and Warrington /25/ have proposed that this results from the migration of subgrain boundaries. It has often been observed that subgrain boundaries migrate during deformation. Their relative strain contribution $A_m = d\varepsilon_m/d\varepsilon$ is of order 0.1 in the steady state and goes up to about 1 shortly after a large reduction in stress when net motion of free dislocations is suppressed /26,27/. A boundary dislocation segment per volume, $d\rho_b$, migrating the distance between boundaries of opposite sign, creates a strain $d\epsilon_m = (b/M)n_b w d\rho_b$ and reduces the boundary dislocation density by $d\rho_b^- = 2d\rho_b$. The relative decrease in density $d\rho_b^-/\rho_b$ equals the relative increase dw/w in subgrain size at constant boundary-dislocation spacing s. Therefore, the relative increase in subgrain size with strain occurs at the rate /28/:

$$\frac{d \ln w}{d\epsilon} = \frac{A_m M}{2 n_b \Theta} \quad (9)$$

Fig. 5 shows measured rates $d \log w/d\varepsilon$. They are plotted as a function of $w^\infty/w_o \sim \sigma_o/\sigma$, where w_o is the initial subgrain size (introduced at steady-state deformation at σ_o) and w^∞ is the new steady-state value of the subgrain size at the reduced stress σ. Fig. 5 contains data from various sources for different materials (Al: /33-35/, Fe: /36/, LiF: /26/, NaCl: /37/, AlZn: /13/, AlMnMg: /13/ and X20CrMoV121: /28,38,39,40/). It is seen that for large stress reductions (large w^∞/w_o) most data for pure materials lie close to the growth rate $d \log w/d\varepsilon$ predicted for $A_m = 1, \theta = 0.5°, n_b = 3$. With decreasing degree of stress reduction $d \log w/d\varepsilon$ decreases continuously towards 0 in the limit of $\sigma = \sigma_o$ (no stress reduction), as expected. The growth rates of 12%Cr-steel are smaller than those for pure materials by a factor of 3. This can be rationalized by higher misorientation θ than in the pure materials due to the higher stresses involved (> 160 MPa compared to < 20 MPa). We conclude that dynamic subgrain coarsening of pure as well as hardened materials can be rationalized in terms of subgrain boundary migration.

So far, we have assumed that the steady state of the dislocation structure is solely due to dislocation reactions, including reactions with subgrain boundaries. However, at high temperatures and high stresses this

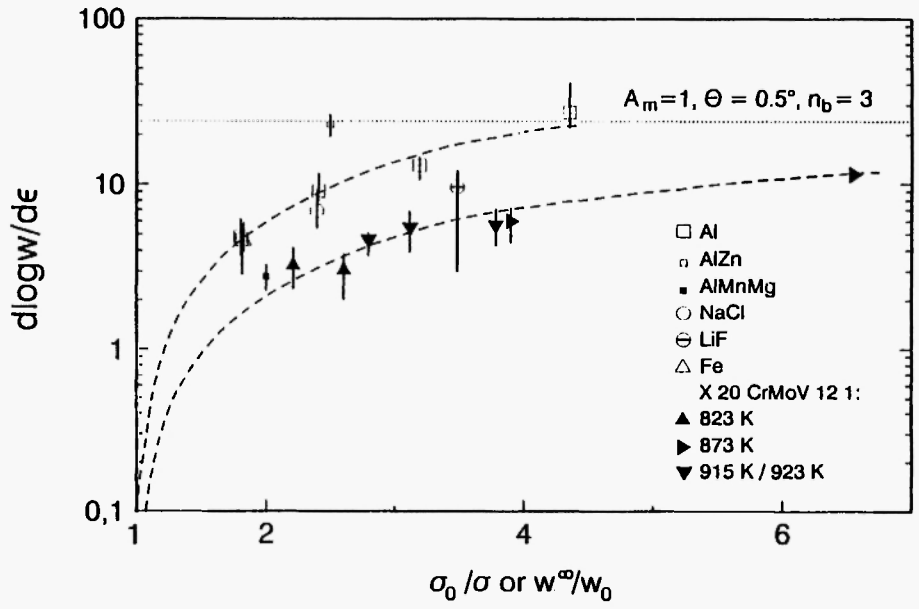

Fig. 5: Rate $d \log w/d\varepsilon$ of dynamic subgrain growth with strain as a function of the factor of stress reduction (σ_o: initial stress, σ: reduced stress).

may no longer be true, because grain boundaries come into play. The sweeping of the deformed material by grain boundaries is an alternative process of structural restoration which is quite common in hot working /41/ and leads into a steady state, where interaction between dislocations (recovery) and interaction of dislocations with moving grain boundaries (recrystallization) combine in compensating dislocation generation during deformation. Even in materials with high stacking fault energies like polycrystalline Aluminium, where recovery is relatively easy, extensive dynamic grain growth is found at high temperatures /4,42/ at constant stress and dynamic recrystallization can be triggered by a sudden reduction in stress /43/. Pure materials with high stacking fault energy recrystallize dynamically even in the single crystalline state.

3. Kinetics of Deformation

A. Steady State of Deformation

Figs. 6a and 6b show the steady-state creep rates of LiF and bcc Fe, normalized according to Eq. 2, as a function of shear-modulus normalized (normal) stress. Normalization of $\dot{\varepsilon}$ was done with the diffusion coefficient of F in LiF (Fig. 6a) and of Fe in Fe (Fig. 6b) /4/. Also the shear moduli were taken from Frost and Ashby /4/. The results for LiF and Fe are typical for materials of high stacking fault energy /3,29,43/: At stresses below $10^{-4}G$ the creep rate is in good agreement with the prediction of the natural creep law (Eq. 2). At high stresses, however, the steady-state creep rates are distinctly larger than predicted by that law. This phenomenon is called power-law breakdown. It means that the stress dependence of the dislocation velocity is no longer linear at high stresses.

The low-stress data for Fe are supported by those for FeSi. The deviation of the FeSi-data from the natural law below $\sigma = 3 \cdot 10^{-6}G$ has been ascribed to a separate mechanism of creep called Harper-Dorn creep /31/. However, as pointed out in /12,43/, it is not clear whether a new mechanism needs to be invoked. The simplest explanation of Harper-Dorn creep is in terms of Eq. 2, assuming that creep occurs at constant dislocation density so that the apparent stress exponent is reduced from 3 to 1. The dislocation density may be constant because in the range of extremely low stresses and creep

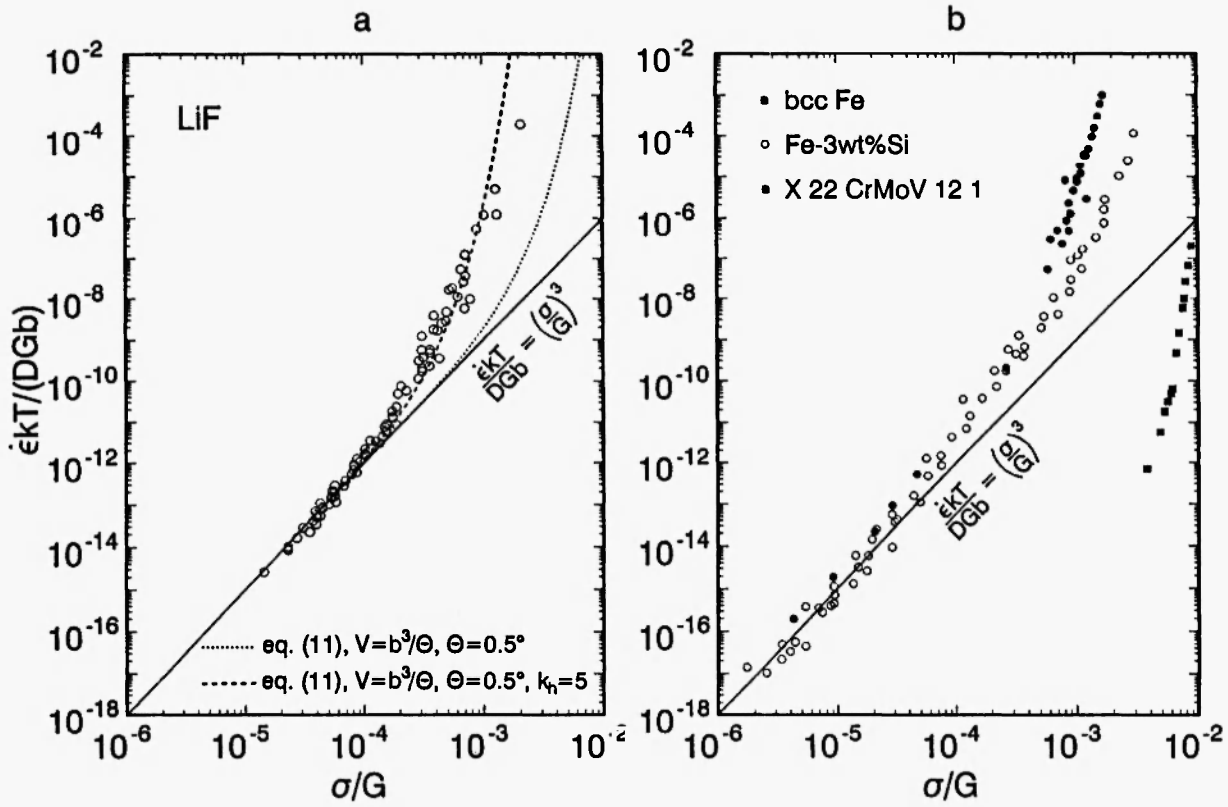

Fig. 6: Relation between normalized strain rate $\dot{\varepsilon}$ and normalized stress σ for steady state deformation of a) pure LiF /29/ and b) pure bcc Fe /3,30/, Fe-3 wt%Si /31/ solid solution and for the point of maximum creep resistance (minimum creep rate) of 12%Cr-steel at 500 °C /32/.

rates, where Harper-Dorn creep is observed, there is not enough strain available in the time of testing for the dislocation density to attend its steady-state value. Note that the steady-state dislocation density is quite low at $\sigma \leq 10^{-6}G$: according to Eq. 2 the average spacing of free dislocations in the steady state should be $\rho_f^{-0.5} \geq 10^6\, b \approx 0.3$ mm) corresponding to a density $\rho_f \leq 10^7/m^2$, which is below the dislocation density typically found in a metallic sample prior to testing. The above explanation of Harper-Dorn creep implies that proper stress-change tests should still yield a steady-state stress exponent of 3. This may be checked.

Solid-solution hardening by Si in FeSi shows up only at the upper right of Fig. 6b, i.e. at low temperatures and high stresses. Here the FeSi-curves deviate from the curve of pure Fe, because increasing $\dot{\varepsilon}$ causes an increasing fraction of the applied stress to be supplied for solute friction. In the limiting case of viscous motion of dislocations surrounded by a cloud of foreign atoms the natural creep law would approximately be fulfilled (with D being the diffusion coefficient for motion of the cloud of solute atoms). This is in fact observed in a number of cases, e.g., that of AlMg /14,45/.

The data for the minimum creep rate $\dot{\varepsilon}_{min}$ of the creep resistant 12%Cr-steel X22CrMoV121 at 500 °C are by far the lowest ones for given stress in Fig. 6b. The reason for this is that this tempered martensite steel is hardened by carbides and subgrains. Note, however, that $\dot{\varepsilon}_{min}$ is not a steady-state creep rate, because the dislocation structure is not in a state of stable dynamic

equilibrium (see next section).

B. Transient Deformation

The transient deformation at constant stress depends on the initial microstructure, which is determined either by the thermal or thermomechanical pretreatment of the material *before* the test or by the predeformation *during* the test. The pretreatment before the test leads to different microstructures in ferritic and austenitic steels. Austenitic steels, like other fcc alloys, usually contain a relatively low initial dislocation density. Their major structural change during creep is densification of the dislocation structure, first by decrease of $\rho_f^{-0.5}$ and followed by subgrain formation /15/. Due to the low initial value of σ_G and the high corresponding initial value of σ^*, dislocations can break away from their clouds of foreign atoms during initial loading. This causes some marked ***instantaneous*** strain, which increases with stress like the strain in a stress-strain-curve at high deformation rate /12,46,47/ and can go up to very high values of 0.6. In Fig. 7a the instantaneous strain due to breaking away is 0.034. With increasing dislocation density and decreasing σ^* the dislocations slow down and are eventually caught again by clouds. Subsequently the subgrain structure forms and $\dot{\varepsilon}$ decreases with ε. The f_{sub}-curve shown in Fig. 7a has been estimated based on the empirical formula for $\varepsilon_{sub,50\%}$ given in section 2.

Ferritic steels undergo the γ-α phase transformation. In the tempered martensite state the microstructure consists of small subgrains and carbides. The volume fraction f_{sub} of material containing subgrains is 1 throughout the transient range of deformation. The subgrain size w gradually approaches the steady-state value corresponding to the applied stress. The carbides grow /38,48,49/. Initially $\dot{\varepsilon}$ is high, because the dislocations introduced during pretreatment rearrange easily. After the minimum of $\dot{\varepsilon}$ the material softens dynamically /39/. As the softening is observed not only in tension, but also in compression (Fig. 7b), it cannot be solely due to internal or external necking, but must be related with other microstructural features like growth of subgrains and carbides /39,49/. It is surprising to note that the exact reason for the softening of simple heat resistant steels during long term creep is not yet clear and cannot be quantitatively described on a convincing microstructural basis. This is a challenge for future work.

C. Deformation at Constant Microstructure

The transient deformation response after a change in stress contains interesting information about the kinetics of dislocation motion. We omit here the attempts to determine an approximate value of the athermal stress component from "dip tests" and concentrate instead on the relationship between σ and the rate of deformation $\dot{\varepsilon}_{cs}$ at constant dislocation structure. The curves shown in Fig. 8 are typical for pure materials. $\dot{\varepsilon}_{cs}$ is a sum of two terms $\dot{\varepsilon}_1$ and $\dot{\varepsilon}_2$ /50/. The term $\dot{\varepsilon}_1$ dominating at high stresses can be ascribed to thermally activated motion of free dislocations over obstacles connected with the dislocation structure. If the obstacles are formed by forest dislocations, the operational activation area $\Delta a = (Mk_BT/b)\partial \ln\dot{\varepsilon}/\partial\sigma$, which can be determined from the slope of the curves in Fig. 8 at $\sigma = \sigma_o$, should contain information on the obstacle spacing. Assuming that the obstacle width is b, the obstacle spacing should be of the order of $\Delta a^*/b$, where $\Delta a^* = 1.5\ \Delta a$ is the true activation area according to Friedel. Δa^* is plotted in Fig. 9. By comparing with Fig. 4 it is seen that $\Delta a^*/b$ is in fact of the order of (and somewhat larger than) the average spacing of dislocations in the subgrain interior, $\rho_f^{-0.5}$. This means that forest dislocations may be the thermal obstacles for free dislocations not only during room temperature work hardening, but also during steady-state creep, as proposed previously /50,51,53/. By increasing the slope of the $\dot{\varepsilon}_1$-curve for Al in Fig. 8 by the factor of 1.5, one obtains the dotted curve for constant "true" obstacle spacing corresponding to the true activation area. The dotted curve falls to $\dot{\varepsilon}_{cs} = 0$ at $\sigma/\sigma_o \approx 0.8$. This means that the thermal stress component is of order of 20% of the applied stress during steady-state deformation at the given conditions.

The $\dot{\varepsilon}_2$-term dominating at low stresses represents the maximum deformation rates measured after the anelastic back flow has ceased. The slow motion of dislocations here is associated with the recovery of the dislocation structure /21/, in particular subgrain growth by migration (see section 2C).

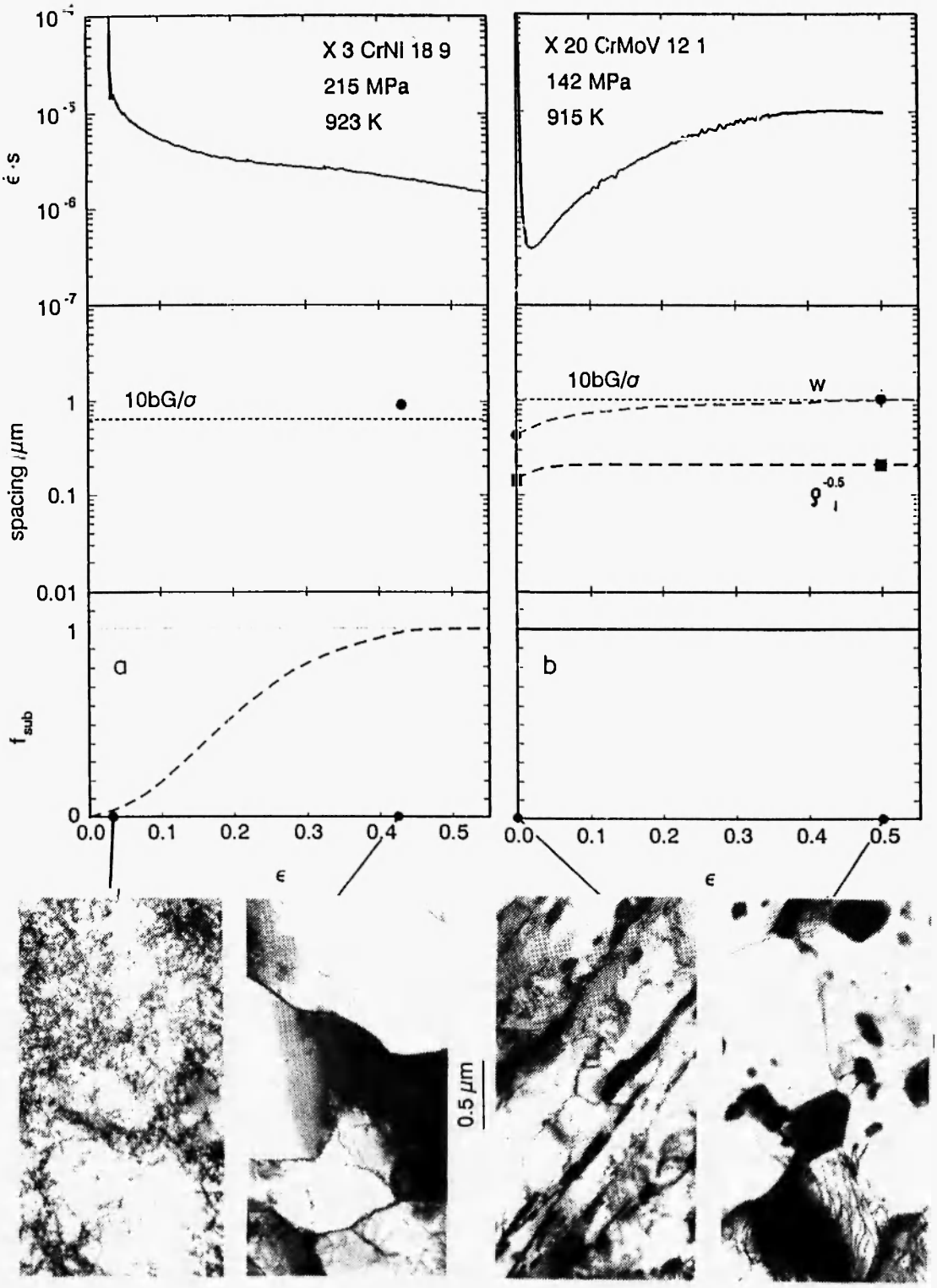

Fig. 7: Creep rate $\dot{\varepsilon}$ and dislocation structure at constant compressive stress as a function compressive strain ε for a) an austenitic /44/ and b) a ferritic steel.

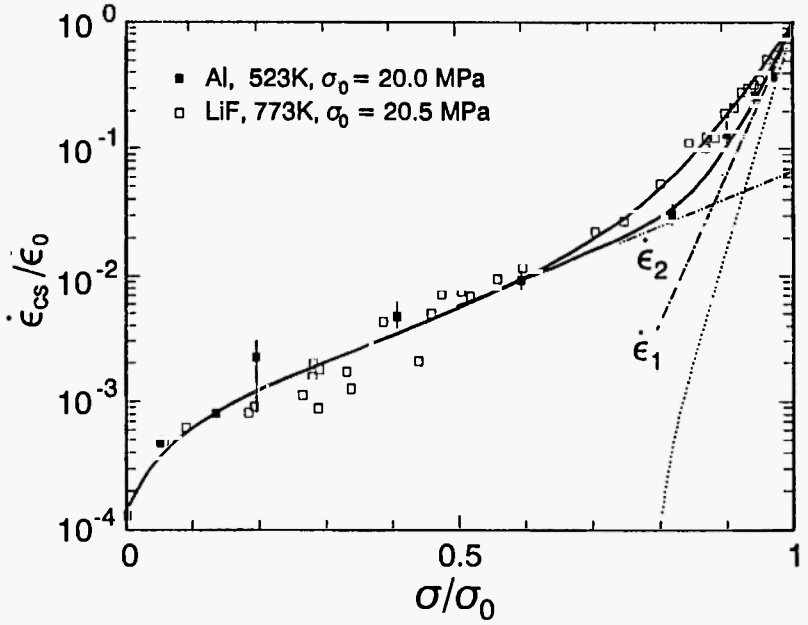

Fig. 8: Relation between strain rate $\dot{\varepsilon}_{cs}$ and stress σ at constant microstructure for Al and LiF /12/. For Al $\dot{\varepsilon}_{cs}$ is decomposed into $\dot{\varepsilon}_1$ and $\dot{\varepsilon}_2$.

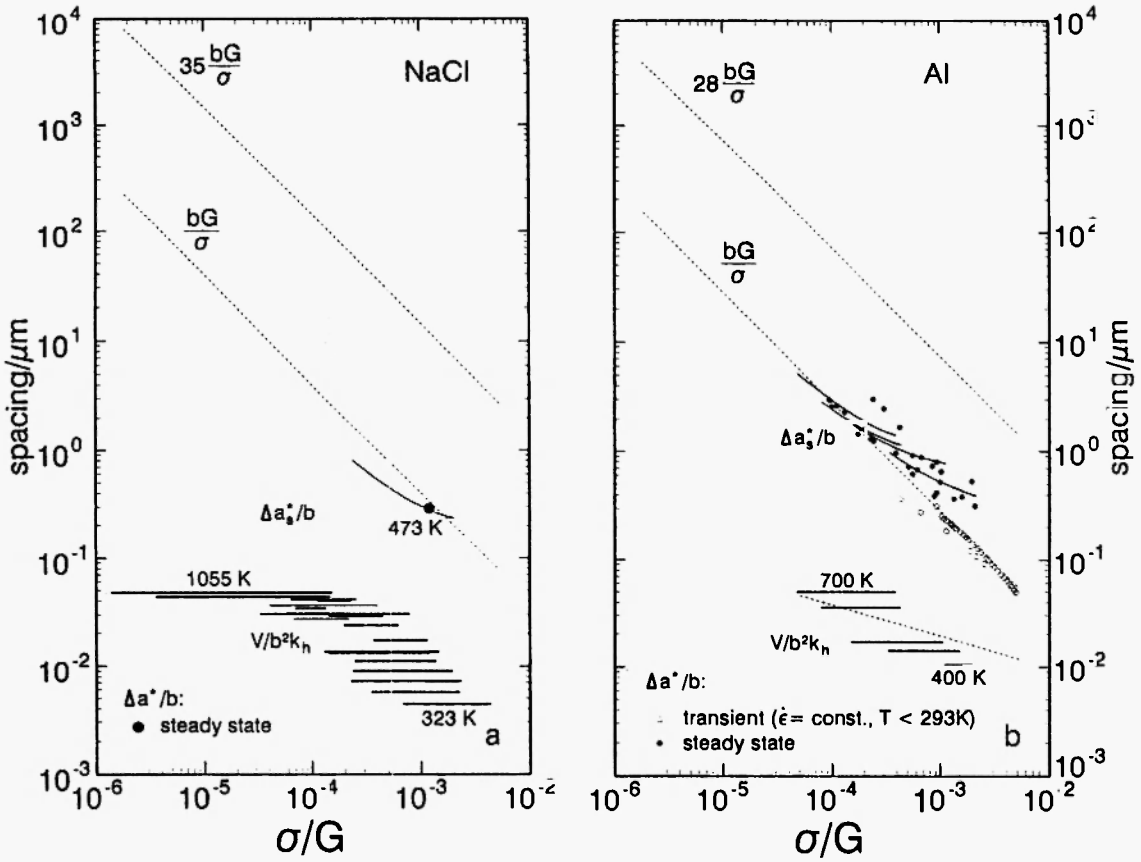

Fig. 9: V/b^2k_h, $\Delta a^*_s/b$ and $\Delta a^*/b$ as a function of shear-modulus normalized stress for a) NaCl /16/ and b) Al /51,52/.

4. Modeling of Deformation

A model of deformation should account for the deviation from the natural law of steady-state deformation ("power-law breakdown", PLB) and the relation between the two different mechanisms of dislocation motion governing glide and recovery. It is well known that the PLB problem can be solved by assuming a stress concentration at the points where emission of vacancies occurs. Barrett and Nix /55/ rationalized this stress concentration in terms of jogged screw dislocations. At the *climbing* jogs stress is concentrated due to *glide*. Therefore the velocity of climb,

$$v_c \propto D \sinh\left(\frac{V\sigma/M}{k_B T}\right) \qquad (10)$$

is no longer proportional to stress as it is the case, if the activation volume $V \approx \Omega$ and the sinh-term can be linearized as it has been assumed in deriving Eq. 2. There are arguments against the applicability of the model /56/. However, Eq. 10 can be derived in an alternative way by considering the migration of subgrain boundaries.

Derby and Ashby /54/ postulated that glide and climb are coupled during migration of a subgrain boundary (Fig. 10a) so that the mechanical work done per atom moved is $V\sigma/M = \Omega(\sigma/M)/\theta \approx b^2 s\sigma/M$. $1/\theta = s/b$ acts as a stress concentration factor. It is of order 100 for typical values of θ. From the definition of A_m (section 2) and the expression for the velocity of subgrain boundary migration /54/, modified in the sense of Eq. 10, one obtains /52/:

$$\dot{\epsilon} = \dot{\epsilon}_m / A_m \propto \frac{D}{A_m s w^2} \sinh\left(\frac{V\sigma/M}{k_B T}\right) \qquad (11)$$

which is identical to the Barrett-Nix formula with respect to the stress and temperature dependence of the steady-state creep rate.

However, it seems doubtful whether long-range stress concentrations of the magnitude of a factor of 100 exist, because it seems probable that they are relaxed by glide (Fig. 10b). Therefore an explanation of the steady-state $\dot{\epsilon}$-σ-relation (11) should be sought in terms of thermally activated glide, where stress concentration is of local nature. In fact, any mechanism of thermally activated dislocation motion with an activation area related to the dislocation spacing in subgrain boundaries and a temperature dependence not too different from that of diffusion can explain the steady-state $\dot{\epsilon}$-σ-relation. As glide is easier than diffusion at low temperatures (and high stresses) it is reasonable to anticipate that with decreasing temperature glide becomes dominant as the controlling process. Mecking et al. /57/ concluded from a comparison of the temperature dependence of the steady-state flow stress for different fcc metals that "dynamic recovery is influenced most significantly by dislocation arrangements that do not require diffusion". Siethoff and Schröter /58/ deduced from an analysis of the σ-ε-curves that steady-state creep in diamond-cubic semiconductors is controlled by cross slip. A detailed proposal of subgrain boundary migration being controlled by cross slip has been made by Caillard /59/.

Fig. 6a shows that the curve calculated from ex-

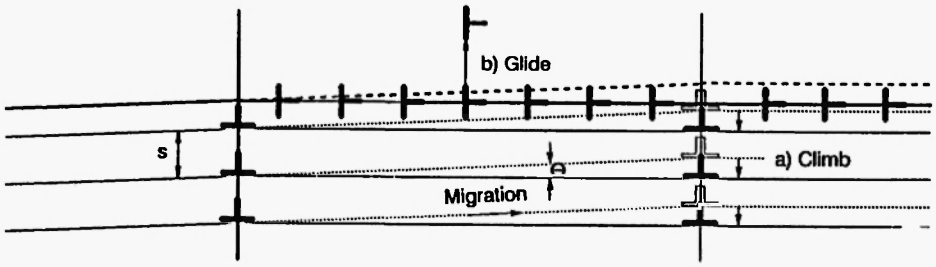

Fig. 10: a: Climb coupled to glide during migration of subgrain boundary with tilt component /54/ and b: Relaxation of incompatibility stresses by glide.

pression (11) (with $V = \Omega/\theta = b^2 s$, $\theta = 0.5°$, $T = 0.9T_m$, T_m: melting point) predicts PLB to occur at $\sigma = 5 \cdot 10^{-4}G$. Experimentally, the PLB is found at $10^{-4}G$. Thus a moderate stress concentration is necessary to explain the experimental results. This can be achieved with the composite model /3,60/. It deals with the flow of free dislocations through the subgrain interior (local creep rate $\dot{\epsilon}_{f,s}$) and the subgrain boundaries (local creep rate $\dot{\epsilon}_{f,h}$), which are regarded as soft and as hard regions, where the stresses σ_s and σ_h are acting, respectively. The total creep rate due to motion of free dislocations is /52/:

$$\dot{\epsilon}_f = f_s\,\dot{\epsilon}_{f,s}(\sigma_s) + f_h\,\dot{\epsilon}_{f,h}(\sigma_h) + f_h(\epsilon_{f,h} - \epsilon_{f,s})$$

$$\sigma = f_s\sigma_s + f_h\sigma_h$$

$$f_s + f_h = 1 \qquad (12)$$

where f_h and f_s are the volume fractions of the hard and soft regions, respectively. It is assumed that the flow of free dislocations through subgrain boundaries by knitting/deknitting at the rate $\dot{\epsilon}_{f,h}$ is controlled by boundary migration (see Caillard /59/):

$$\dot{\epsilon}_{f,h} = f_m\dot{\epsilon}_m. \qquad (13)$$

The combination of Eqs. 12 and 13 leads to the experimentally observed proportionality between $\dot{\epsilon}$ and $\dot{\epsilon}_m$ noting that in the steady state $\dot{\epsilon}_{f,s} = \dot{\epsilon}_{f,h}$ and $f_m = 0$, and that the total strain rate $\dot{\epsilon}$ is the sum of the contributions due to glide of free dislocations $\dot{\epsilon}_f$ and migration of subgrain boundary dislocations $\dot{\epsilon}_m$:

$$\dot{\epsilon} = \dot{\epsilon}_f + \dot{\epsilon}_m. \qquad (14)$$

This type of equation is consistent with the strain rate-stress relation at constant structure (Fig. 8). The observation $A_m \approx 1$ after a large stress reduction (see section 2) simply means that migration of subgrain boundaries makes a major contribution to the creep rate associated with recovery so that $\dot{\epsilon}_2 \sim \dot{\epsilon}_m$ for steady-state dislocation structures.

The stress at subgrain boundaries must now be replaced by $\sigma_h = k_h\sigma$ so that $V = b^2 s k_h$. The curve in Fig. 6a obtained with $k_h = 5$ is seen to well explain the observed PLB behaviour. The values of V/b^2k_h have been determined from the observed steady-state $\dot{\epsilon}$-σ-relations of NaCl and Al at constant temperature assuming $k_h = 5$. Comparison of Figs. 4b and 9b shows that they fall well into the observed range of s-values.

The model described above not only accounts for steady-state creep, but also shows how glide of free dislocations in the subgrain interior and recovery are coupled. Recovery involves the transport of dislocations to sinks /61/. In our picture the sinks are subgrain boundaries containing dislocations of opposite sign and the free dislocations have to be transported by glide through the subgrain boundaries and the subgrain interior until they arrive at a sink. The strain rate in the subgrain interior of pure materials $\dot{\epsilon}_{f,s}$ is formulated in terms of thermally activated glide:

$$\dot{\epsilon}_{f,s} = (b/M)\,\rho_f\,v_{o,s}(T)\,[\exp(b\Delta a_s^*\sigma_s^*/Mk_BT) - 1] \qquad (15)$$

Fig. 9 shows the variation of $\Delta a^*{}_s$ with stress which fits to the observed values of Δa^* and at the same time fulfills the requirement $\dot{\epsilon}_{f,s} = \dot{\epsilon}_{f,h}$. The good agreement between $\Delta a^*{}_s$ and Δa^* means that the model is able to explain the $\dot{\epsilon}$-σ relationships for conditions of steady state as well as constant structure /52/.

When the change of the dislocation structure from the initial state to the final state is taken into account, it is also possible to calculate the transient deformation response of pure materials /52,62/. First efforts to apply the model to calculate the transient $\dot{\epsilon}$-ϵ-curves of strongly solute hardened alloys, by replacing Eq. 15 by an equation appropriate for viscous motion of dislocations with clouds, have yielded promising results for the change in stress exponent of the steady-state creep rate and the change in transient creep from normal to inverted type /12/.

We conclude that a model based on *two* mechanisms of dislocation motion in the soft and the hard

regions of the material, which are coupled by internal stresses, is consistent with the dynamics of creep and the dislocation structure of pure materials and simple alloys. It offers the chance to calculate creep for steady state as well as transient conditions, after the detailed values of the parameters of the model for a specific material have been obtained by a suitable fitting procedure. The fitting must be based on the results of long-term creep tests as long as the degradation of particle hardening and the growth of pores in creep resistant materials are still insufficiently known.

Acknowledgements

We wish to thank the Bundesminister für Forschung und Technologie, the Bundesminister für Wirtschaft and the Verein Deutscher Eisenhüttenleute for their financial support of this work.

References

1. Sherby, O.D. and Burke, P.M., *Progr. Mater. Sci.*, **13**, 325-390, 1967.
2. Bird, J.E., Mukherjee, A.K. and Dorn, J.E., in: Quantitative Relation between Properties and Microstructure, Israel University Press, Jerusalem, 255-342, 1969.
3. Nix, W.D. and Ilschner, B., in: Proc. 5th Int. Conf. on the Strength of Metals and Alloys (ICSMA 5), P. Haasen, V. Gerold and G. Kostroz (Eds.), Pergamon Press, Oxford, 1503-1530 (1980).
4. Frost, H.J. and Ashby, M.F., Deformation-Mechanism Maps, Pergamon Press, Oxford.
5. Weertman, J., in: Rate Processes in Plastic Deformation of Materials, J.C.M. Li and A.K. Mukherjee (Eds.), American Society for Metals, 315-336, 1975.
6. Alexander, H. and Haasen, P., *Solid State Physics*, **22**, 27, 1968.
7. Blum, W. and Reppich, B., in: Creep Behaviour of Crystalline Solids, B. Wilshire and R.W. Evans (Eds.), Pineridge Press, Swansea, 83-135, 1985.
8. Reppich, B., in: Plastic Deformation and Fracture of Materials, H. Mughrabi (Ed.), Vol. 6 of Materials Science and Technology, R.W. Cahn, P. Haasen and E.J. Kramer (Eds.), VCH Verlagsgesellschaft, Weinheim, 1992.
9. Riedel, H., Fracture at High Temperatures, Springer, Berlin (1987).
10. Hasegawa, T., Karashima, S. and Hasegawa, R., *Metall. Trans.*, **2**, 1449-1455 (1971).
11. Carrard, M. and Martin, J.L., in: Creep and Fracture of Engineering Materials and Structures, B. Wilshire and R.W. Evans, (Eds.), Pineridge Press, Swansea, 27-38 (1984).
12. Blum, W., in: Plastic Deformation and Fracture of Materials, H. Mughrabi (Ed.), Vol. 6 of Materials Science and Technology, R.W. Cahn, P. Haasen and E.J. Kramer (Eds.), VCH Verlagsgesellschaft, Weinheim (1992).
13. Blum, W., in: Hot Deformation of Aluminium Alloys, G. Langdon, H.D. Merchant, J.G. Morris and M.A. Zaidi (Eds.), The Minerals, Metals & Materials Society, Warrendale, 181-209 (1991).
14. Oikawa, H. and Langdon, T.G., in: Creep Behaviour of Crystalline Solids, B. Wilshire and R.W. Evans (Eds.), Pineridge Press, Swansea, 33-82 (1985).
15. An, S.U., Wolf, H., Vogler, S. and Blum, W., in: Creep and Fracture of Engineering Materials and Structures, B. Wilshire and R.W. Evans (Eds.), The Institute of Metals, London, 81-95 (1990).
16. Vogler, S., Dr.-Ing. thesis, University of Erlangen-Nürnberg (1992).
17. Raj, S.V. and Pharr, G., *Mater. Sci. Eng.*, **81**, 217-237 (1986).
18. Matucha, K.-H., *Phys. Stat. Sol.*, **26**, 291-310 (1968).
19. Ambrosi, P. and Schwink, W., in: Proc. 5th Int. Conf. on the Strength of Metals and Alloys (ICSMA 5), P. Haasen, V. Gerold and G. Kostorz (Eds.), Pergamon Press, Oxford, 29-33 (1980).

20. Morris, M., Masson, D., Senior, B. and Martin, J.L., *Scripta metall.*, **17**, 687-692 (1983).

21. Kocks, U.F., in: Proc. of the Conf. at the 50th Anniversary Meeting on Dislocations and Properties of Real Materials, The Institute of Metals, London, 125-143 (1985).

22. Matucha, K.-H., Franzbecker, W. and Wilkens, M., *Phys. Stat. Sol.*, **33**, 493-497 (1969).

23. Strunk, H., *Mater. Sci. Eng.*, **27**, 225-238 (1977).

24. Singer, R., Blum, W. and Nix, W.D., *Scripta metall.*, **14**, 755-760 (1980).

25. Exell, S.F. and Warrington, D.H., *Phil. Mag. A*, **26**, 1121-1136 (1972).

26. Biberger, M., Dr.-Ing. thesis, University of Erlangen-Nürnberg (1989).

27. Biberger, M. and Blum, W., *Phil. Mag. A* (1992).

28. Blum, W. and Straub, S., *Steel Research*, **62**, 72-74 (1991).

29. Biberger, M. and Blum, W., *Scripta metall.*, **23**, 1419-1424 (1989).

30. Uvira, J.L. and Jonas, J.J., *Trans. AIME*, **242**, 1619-1626 (1968).

31. Ruano, O.A., Wadsworth, J. and Sherby, O.D., *Scripta metall.*, **22**, 1907-1910 (1988).

32. Kloos, K.H., Granacher, J. and Oehl, M., *Mat.-wiss. u. Werkstofftech.*, **21**, 265-274 (1990).

33. Ferreira, I. and Stang, R.G., *Mater. Sci. Eng.*, **38**, 169-174 (1979).

34. Ferreira, I. and Stang, R.G., *Acta metall.*, **31**, 585-590 (1983).

35. Soliman, M.S., Ginter, T.J. and Mohamed, F.A., *Phil. Mag. A*, **48**, 63-81 (1983).

36. Immarigeon, J.-P. A. and Jonas, J.J., *Acta metall.*, **19**, 1053-1061 (1971).

37. Eggeler, G. and Blum, W., *Phil. Mag. A*, **44**, 1065-1084 (1981).

38. Nilsvang, N., Doctoral Thesis No. 815, Ecole Polytechnique Fédérale de Lausanne (1989).

39. Blum, W. and Straub, S., in: Creep Czechoslovakia 1991, Proc. of the VIIIth Int. Symp. on Creep-Resistant Metallic Materials, Sept. 17-19, Zlín, CSFR, 178-185 (1991).

40. Straub, S., current research.

41. McQueen, H.J. and Jonas, J.J., in: Plastic Deformation of Materials, R.J. Arsenault (Ed.), Vol. 6 of Treatise on Materials Science and Technology, Academic Press, New York, 393-493 (1975).

42. Servi, I.S. and Grant, N.J., *Trans. AIME*, **191**, 917-922 (1951).

43. Straub, S. and Blum, W., *Scripta metall. mater.*, **24**, 1837-1842 (1990).

44. Großhäuser, M., Dipl.-Ing. thesis, University of Erlangen-Nürnberg (1991).

45. Nakashima, H., in: Creep and Fracture of Engineering Materials and Structures, B. Wilshire and R.W. Evans (Eds.), The Institute of Metals, London, 41-50 (1990).

46. Blum, W., in: Werkstoffverhalten und Bauteilbemessung, E. Macherauch (Ed.), DGM Informationsgesellschaft, Oberursel, 185-207 (1986).

47. Zauter, R., Petry, F., Christ, H.-J. and Mughrabi, H., *Mater. Sci. Eng.*, **A124**, 125-132 (1990).

48. Eggeler, G., Ilschner, B. and Nilsvang, N., in: Proc. 9th Int. Conf. on the Strength of Metals and Alloys (ICSMA 9), D.G. Brandon, R. Chaim and A. Rosen (Eds.), Freund Publishing House, London, 351-358 (1991).

49. Eggeler, G., *Acta metall.*, **37**, 3225-3234 (1989).

50. Blum, W., Rosen, A., Cegielska, A. and Martin, J.L., *Acta metall.*, **37**, 2439-2453 (1989).

51. Blum, W., Vogler, S., Biberger, M. and

Mukherjee, A.K., *Mater. Sci. Eng.*, **A112**, 93-106 (1989).

52. Vogler, S. and Blum, W., in: Creep and Fracture of Engineering Materials and Structures, B. Wilshire and R.W. Evans (Eds.), The Institute of Metals, London, 81-95 (1990).

53. Nakayama, G.S. and Gibeling, J.C., *Scripta metall. mater.*, **24**, 2031-2035 (1990).

54. Derby, B. and Ashby, M.F., *Acta metall.*, **35**, 1349-1353 (1987).

55. Barrett, C.R. and Nix, W.D., *Acta metall.*, **13**, 1247-1258 (1965).

56. Caillard, D. and Martin, J.L., *Revue Phys. Appl.*, **22**, 169-183 (1987).

57. Mecking, H., Nicklas, B., Zarubova, B. and Kocks, U.F., *Acta metall.*, **34**, 527-535 (1986).

58. Siethoff, H. and Schröter, W., *Z. Metallkde.*, **75**, 475-491 (1984).

59. Caillard, D., *Phil. Mag. A*, **51**, 93-106 (1985).

60. Mughrabi, H., in: Proc. 5th Int. Conf. on the Strength of Metals and Alloys (ICSMA 5), P. Haasen, V. Gerold and G. Kostorz (Eds.), Pergamon Press, Oxford, 1615-1633 (1980).

61. Kocks, U.F., *J. Eng. Mater. Tech.* (ASME-H), **98**, 76-85 (1976).

62. Vogler, S., Wegerer, T., Brandner, G. and Blum, W., in: Proc. of the 9th Int. Conf. on the Strength of Metals and Alloys (ICSMA 9), D.G. Brandon, R. Chaim and A. Rosen, Freund Publishing House, London, 569-576 (1991).